Physics-Based Modeling of Power Converter Drive System for Evaluation of Electromagnetic Compatibility

M. R. Barzegaran, A. Nejadpak, Student ACES, and O. A. Mohammed, Fellow ACES

Energy Systems Research Laboratory, ECE Department
Florida International University, Miami, FL. 33174, USA
mohammed@fiu.edu

Abstract ─ In this paper, detailed physics-based modeling of a power converter drive is proposed. The 3D finite element (FE) modeling of a power inverter was developed and analyzed. An approach in physical modeling of the switching activity of the inverter in FE is proposed. In addition, the solver was modified and implemented for analyzing nonlinear materials in time-harmonic cases to achieve faster computation. The frequency response analysis was also implemented in simulation and measurements at various locations from the source. The numerical simulation provided the exact field solution at any given distance and defined the correlation between the electromagnetic fields generated by each of these components. The importance of this work is to facilitate the ability to evaluate the stray electromagnetic field levels used for evaluating EMC compliance at the design stage. In addition, the recognition of a failure condition inside each component of the system by observing the fields is another important contribution of this work. The optimum operation of the system components for lower EMI and optimum design of related shielding for EMC evaluation studies are added benefit of this work.

Index Terms ─ FE analysis, low frequency EMC analysis, power electronics drives.

I. INTRODUCTION

With the increased development and utilization of power electronic drives, the evaluation of low frequency stray electromagnetic fields (DC to hundreds of kHz) in these devices becomes necessary. Power electronic drives have an electric system of significant power consisting of power converters, electric motors and electric loads. This is in addition to all connecting wires and cables which are usually located in close proximity within the systems. For example, in electric vehicles as an important application of power electronic drives, it is a common practice to place the battery stack as far as possible from the bodywork to reduce the risk of battery damage. This arrangement implies placing them just under the seats of the vehicle. It follows that during acceleration or deep regenerative braking, there might be currents in the hundreds of amperes circulating a few centimeters away from the passengers [1]. In addition to the effect of the stray field into the environment, when harmonic current of low order is emitted into a network, the voltage is distorted reducing the voltage quality. The level of voltage distortion is dependent on the network strength. Similarly, high frequency current harmonics may cause the voltage harmonics in the network. As a harmonics effect, the current harmonics may cause overheating of, e.g., neutral conductors and capacitors in three-phase systems. Also, the voltage harmonics may upset the electronics, e.g., due to multiple zero crossings; therefore, the loading capability of induction machines may be reduced [2].

The equivalent circuit modeling of power electronic drives is not applicable for studying the radiated emission in the three dimensional areas around the drive. Therefore, the physics based modeling is proposed in this paper to evaluate the stray field in the three dimensional space around the devices. In addition, the material properties of the devices and shape representation were investigated in this modeling process. On the other hand, time-varying electric and magnetic fields generate MMFs and EMFs that can sustain the fields that compromise the flux. Also, the currents and voltages in electric power systems are time-varying, which causes stray electromagnetic fields. Therefore, there is a need to model the EMI generated by these systems to develop designs meeting EMC standards.

Several studies were performed in the area of radiated low frequency electromagnetic field (EMF) analysis of power electronic devices [3]-[8]. In [3], some general principles on how to allocate responsibilities between the power grid and connected equipment were investigated with the aim to achieve electromagnetic compatibility in electric power systems. It was shown, in this paper, that in medium and high voltage systems, in absence of comprehensive equipment emission and immunity standards, it is

Submitted On: September 22, 2013
Accepted On: September 24, 2014

suggested that the grid responsible party provides relevant data such as on voltage dips to the party responsible for connecting equipment to the grid. Some studies have dealt with the impact of stray EMFs on the environment including humans and the operation of devices [4]. This test is implemented from very low frequencies 5 Hz to medium frequencies 300 kHz. Both magnetic and electric fields are tested using gauss meters and electric field meters. On the other side, other studies were conducted to implement attenuators and shielding of the conducted and field bound EMI [5], [6]. Akagi, *et al*., focuses on a line EMI filter and its combination with a motor EMI filter, along with their effects on attenuation of conducted emission voltage. Furthermore, the effectiveness of an EMI filter configuration when the filter is applied to the motor was discussed [5]. In [6], EMI noises generated in the power converter and diffused on the surface of conductors are targeted to be controlled. Consequently, a new approach based on distributed constant circuit theory along with multilayer power printed circuit technology was used.

For developing a model, the equivalent source representation as well as the physics based modeling were studied. Aouine, *et al*., designed high and low frequency models of the converter for magnetic near field by using modeling switching parts by circular magnetic dipoles [7]. Moreover, the physics based modeling of the power electronic drives in low frequency EMF was studied in [8]-[11]. In [8], the optimum equivalent source modeling along with the physics based modeling of an AC motor was analyzed. The idea of loops was enhanced based on optimization methods. In addition to the implementation of the physics based modeling to machines, this type of modeling was also utilized for the power converter switches for the study of the conducted EMI [11]. Since the conducted EMI mostly exist on printed circuit boards (PCB), the FE model of the PCB was studied. Also, the optimization of EMI performance was accomplished in terms of component placement on the PCB [11].

There is a need to have a physics based model, with all details, for the various system components to include the physical effects of stray fields such as superposition and shielding. However, this model has some issues such as the problem of fast switching of the IGBTs and nonlinear commutation curves. Hence, in this paper, the three dimensional full finite element modeling of a typical power electronic drive at low frequency is analyzed. The identified issues with the proposed resolutions are explained. The frequency response analysis of the power converter drive was implemented in the simulation as well as in the experimental setup in two cases of setup, one with an AC load and the other with an induction motor, as a dynamic load. The results of these two cases were compared and their application in EMC study was discussed.

II. STRAY LOW FREQUENCY FIELD CALCULATION

Assuming an electric component as consisting of a series of a large number of infinitesimally short conducting elements, each of such elements is so short that the current may be considered uniform over its length. The field of the entire component may be obtained by integrating the fields from all these differential elements, with the proper magnitude and phases taken into account. It is proposed to review the radiation properties of such a differential element, named as a short dipole for low frequency propagation.

A short dipole, also called a Hertzian dipole, is a thin, linear conductor whose length l is very short compared with the wavelength λ, l should not exceed λ/50 which is not an issue for low frequency analysis. The wire which is oriented along the z-direction as shown in Fig. 1, carries a sinusoidally varying current $i(t) = I_0 \cos\omega t$, where I_0 is the current amplitude.

Based on the Biot-Savart law and Ampere's law for time-varing volume current, the retarded magnetic potential in phasor domain is:

$$\mathbf{A} = \frac{\mu}{4\pi}\int_v \frac{\mathbf{J}e^{-jkR}}{R}dv, \tag{1}$$

where J is the current density distribution through volume v observed at the p point with the R distance and

$$k = \frac{\omega}{\upsilon_p}, \tag{2}$$

is the wavenumber of the propagation medium and υ_p is the velocity of propagation in the medium between the charge distribution and observation point [12].

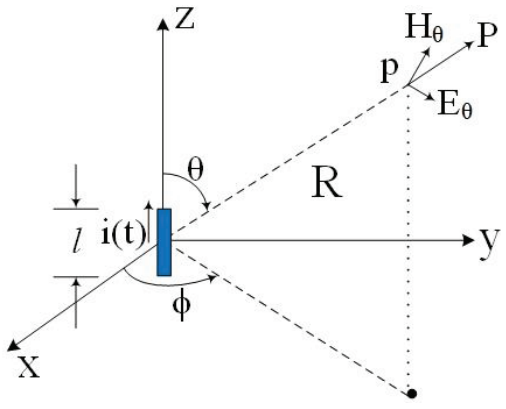

Fig. 1. The electric dipole antenna (the Hertzian dipole).

The time-variant currents and the potential in (1) will lead to an inconstant field with Maxwell equation. The reason is that the time-variant fields give rise to wave propagation. According to which the effect of the source current at a given value of time is felt at a distance R from the origin after a time delay of R/υ_p. Conversely, the effect seen at a distance R from the origin at time t is due to the current existing at the origin at an earlier time (t- R/υ_p). Thus, for the time-varying current element $I_0\, dl\, \cos\omega t\, a_z$ situated at the origin, the magnetic vector potential is given by:

$$\mathbf{A} = \frac{\mu I_0\, dl}{4\pi R}\cos(\omega t - \beta R)\mathbf{a}_z\,, \tag{3}$$

where β is R/υ_p, the phase constant. The magnetic field **H** due to the Hertzian dipole is given by:

$$\mathbf{H} = \frac{I_0\, dl \sin\theta}{4\pi}\left[\frac{\cos(\omega t - \beta R)}{R^2} - \frac{\beta \sin(\omega t - \beta R)}{R}\right]\mathbf{a}_\phi . \tag{4}$$

Equation (4) represents the radiated magnetic field due to the Hertzian dipole [13]. Using Maxwell's curl equation for **H** with **J** set equal to zero in view of perfect dielectric medium, the radiated electric field due to the Hertzian dipole would be given by:

$$\mathbf{E} = \frac{2I_0\, dl\cos\theta}{4\pi\varepsilon\omega}\left[\frac{\sin(\omega t - \beta R)}{R^3} + \frac{\beta\cos(\omega t - \beta R)}{R^2}\right]\mathbf{a}_R + \frac{I_0\, dl\sin\theta}{4\pi\varepsilon\omega}\left[\frac{\sin(\omega t - \beta R)}{R^3} + \frac{\beta\cos(\omega t - \beta R)}{R^2} - \frac{\beta^2\sin(\omega t - \beta R)}{R}\right]\mathbf{a}_\theta . \tag{5}$$

The stray field of a complex model with thousands of dipoles, such as the proposed drive, needs the calculation of the field of each of these dipoles using equations (4) and (5) as well as a vigorous field calculated by using a numerical technique such as the FE method.

The proposed model was accurately built in FE in which the above equations are calculated by modifying the default equations for obtaining electric and magnetic fields. The conductors are modeled as wires, which are modified from volumetric model into linear model, while their magnetic and electric flux density kept constant [CEFC]. The other components which have effect on radiated fields, are mainly switches and capacitors, which are modelled in 3D, but with some modifications that are explained in the following section.

III. SIMULATION AND MEASUREMENT

The proposed setup consists of an inverter, an induction machine, connecting cables and an AC load. The study was divided into two cases for further investigation. The converter connected to an AC load as the case 1 and converter connected to an induction motor as case 2. Each study was discussed along with its application as follows:

Case 1: Converter connected to the load

The proposed full finite element model for the first case is shown in Fig. 2. This electronic drive consists of an inverter, AC load and the armored connection cable. The details of the devices are identified in Table 1.

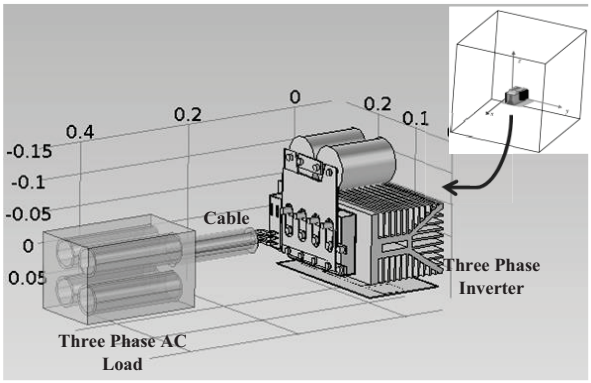

Fig. 2. The prototype of the inverter, load and the connection cable.

Table 1: The details of the components in the tested setup

Component	Characteristics
Inverter	Three-phase, 5.5 kW, Switching frequency: 5-kHz, Switching algorithm: SVM, Length: 30-cm, Width: 30-cm, Height: 25-cm, Nominal voltage: 320-V, Amp: 20-A
Electric load	3-kW AC load
Connection cable	XLPE, Diameters: Cross-sectional area: 1000 mm^2, Thickness of insulation: 2.8 mm, Nominal thickness of pvc sheath: 2.4 mm, Overall diameter: 51 mm, insulated and armored PVC sheathed cable

The schematic of the inverter's circuit is shown in Fig. 3. In this simulation, the IGBT module was operated for a relatively low switching frequency to illustrate the behavior of the circuit. In the PWM inverter of Fig. 3, the duty cycle ratio of the input signal to the IGBT gate drivers is varied using the space vector PWM technique to produce a 60-Hz sinusoidal variation of the RL load current [14].

The operation of the inverter was divided into six sections. During the first $\pi/3(rad)$ of 60-Hz inverter

operation, IGBTs S_{ap}, S_{bn} and S_{cn} are switched on while the others are in the off state. This process changes in a way to track the reference voltage as [14]:

$$V_{ref} = \frac{3}{2}(V_a + \alpha V_b + \alpha^2 V_c), \quad \alpha = e^{j\frac{2\pi}{3}}. \tag{6}$$

The inverter operation during other sequences of the 60-Hz reference sine wave is similar to the aforementioned sequence, except that the opposite phase of the bridge is switched on and off. The sinusoidal variations of the duty cycle ratios for each phase were specified by comparing triangular waveforms to the magnitude of the sinusoidal reference signal. When the value of the reference sine wave is larger than the value of the upper triangle wave, S_{ap} is switched on; otherwise, it must be off. The same procedure goes within the other IGBTs as well. Figure 4 shows the simulated load current for the space vector PWM (SV-PWM) operation.

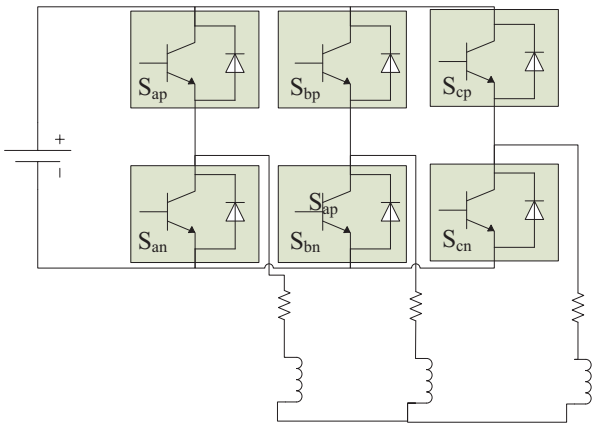

Fig. 3. Schematic of six switch inverter circuit, [17].

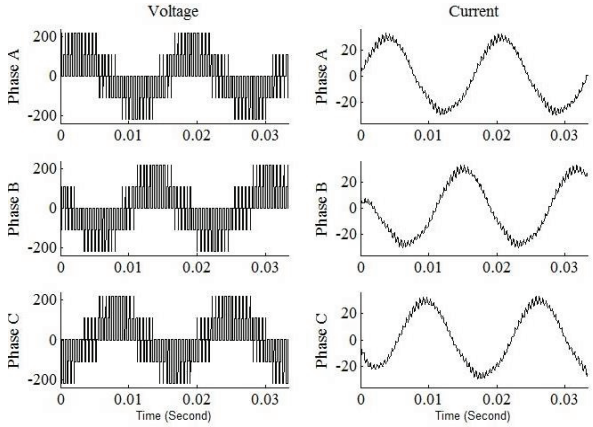

Fig. 4. Line current and voltage in the case of SVPWM.

To model the IGBT switches of the inverter for signature studies, the switches must be considered OFF for a moment of time and then it must be considered ON for the next time instant. This shift occurs based on the switching frequency of the converter. In order to do this in FE simulation, the plate between the load and the positive bus, shown in Fig. 5, is considered a conductive plate for the switch-ON case. Subsequently, this plate is considered a non-conductive plate for the switch-OFF case. This alteration of the conductivity of the plate occurs 5000 times in a second due to the switching frequency (5 kHz).

As mentioned earlier, time-harmonic solution method is being used. Therefore, the transient conditions of the inverter and machines are not considered. The base is on the steady-state condition of a power train. In order to apply this condition in time-harmonic solvers, the model was being captured for the moments of ON and OFF individually and finally the results of the period was accumulated. Since the simulation time would increase dramatically if all time-instants of a time period was considered, hundred time instants are measured.

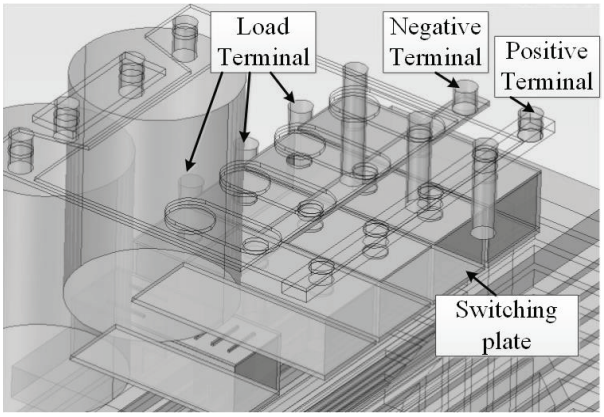

Fig. 5. Physical model of the inverter switches.

The simulation was computed in six hours with about one million elements including face, line and node meshes in the model with six million degrees of freedom. The large number of elements is necessary because of the very small surfaces, edges and lines of the critical part of inverter and cable, as shown in Fig. 6. The details of FE modeling is reflected in [21]-[23]. The simulation was implemented in a fast computer with 192 GB ram and 16 core Intel Xeon 3.47 GHz CPU.

Since there are two cases in this study, it was decided to define two types of results. In case 1, the generated fields of the system on three different surfaces at a distance in space are considered as the result, and in the case 2, the harmonics of the fields and the frequency responses are investigated. Hence, in this case, the generated stray magnetic and electric fields

are obtained in three dimensions at a given distance in both switching circumstances.

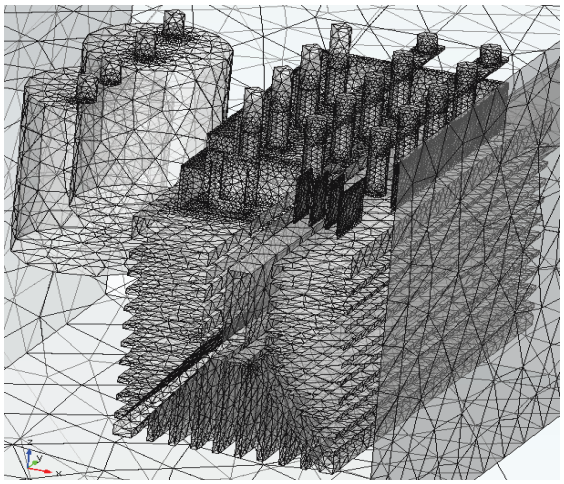

Fig. 6. Mesh pattern of the modeled inverter.

Figures 7 (a) and (b) show that, turning on and off the switches have the effect only on the amplitude of the magnetic field density and the spatial distribution of the stray magnetic field on the slices doesn't change significantly. This is due to the presence of the AC load which is discussed further. On the other hand, the electric field which is shown in Fig. 8, illustrates that when the switches turn on, the electric field in two lateral planes, XY-plane, YZ-plane, increases while the field in the XZ-plane decreases. The increase of the electric field, in these planes, is due to the flow of current in the switches. It is also due to the creation of a current loop and its reduction is because of the superposition which is, suppression in this case. The suppression occurs due to the propagation of fields into the other conductive parts of the devices in vicinity; therefore, the stray field induced from the imposed conductive parts decreases. The reason of the suppression is the inverse direction of the induced field due to Lenz's law [15]. Therefore, the induced stray field is subtracted from the main stray field and the total field decreases as in Fig. 8 (a).

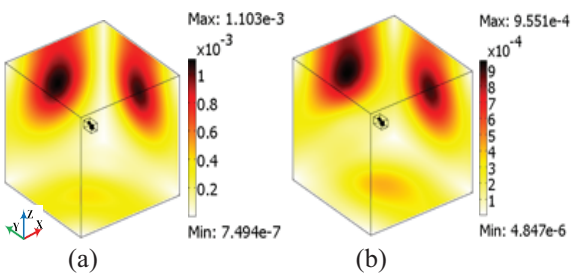

Fig. 7. Stray magnetic field density of the system: (a) IGBT switched on, and (b) IGBT switched off (μT).

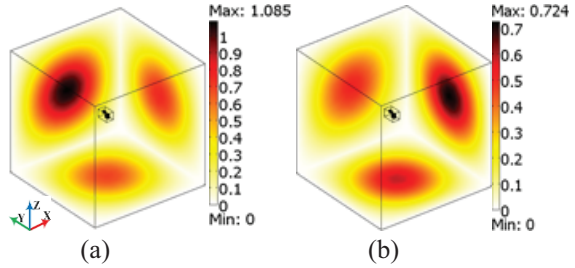

Fig. 8. Stray electric field of the system: (a) IGBT switched on, and (b) IGBT switched off (μV/m).

To recognize which element of the setup has more effect on the total field, the stray magnetic field of each component in this setup were analyzed individually to observe their spectrum and compare it with the overall fields. The results are shown in Figs. 9 (a)-(d). Comparing Fig. 9 (c) with Fig. 9 (a) and Fig. 9 (b), while only the load is switched ON, the stray magnetic field has a higher value in comparison with Fig. 9 (a), (b) and the total field was affected by it (compare Fig. 9 (c) with Fig. 9 (d)). The reason is that the AC load has bigger conductive elements including iron and copper materials compared to the other elements in the setup.

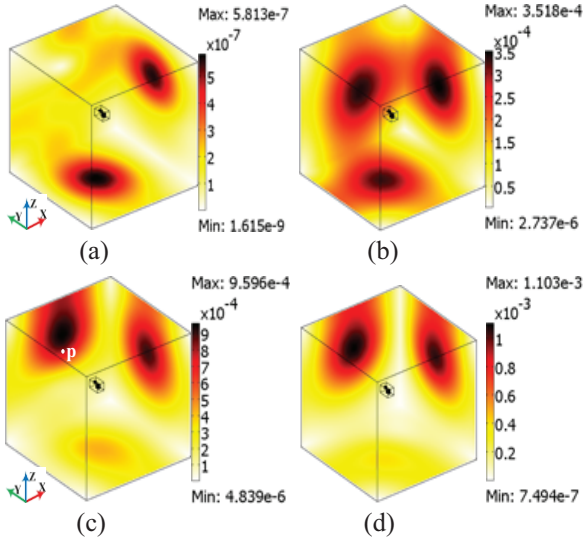

Fig. 9. Stray magnetic field density of the system (μT): (a) only the cable is switched on, (b) only the inverter is switched on, (c) only the load is switched on, and (d) the whole system is switched on.

In order to investigate the effect of superposition, the generated field of a random point (p) of the figures, shown in Fig. 9 (c), can be used. For instance, the values of a point of the three cases (0, 5 m, 0) of Fig. 9, Fig. 9 (a)-Fig. 9 (c), are aggregated. The result is $1.31e^{-3}$ (μT) while the overall maximum point is $1.10e^{-3}$ (μT), as shown in Fig. 9 (d). This can be due to the

dissimilarity of permeabilities and conductivities of the elements of the model. If the resistance of an element is less than another element in the vicinity while there is no shield between them, the EMF will be induced from the component with less conductivity into the one with higher conductivity [16]. As mentioned above, due to Lenz's law, the field radiated from the induced EMF will be the opposite of the main field. Therefore, the overall field will be less than the aggregation of the fields.

Case 2: Converter connected to the motor

In this case, the inverter is connected to an induction motor. The aim of this case is investigating the radiation of the harmonic fields from the inverter while the distance and the speed of the motor change. The parameters of the induction motor are: 5.5-kW, 3-phase, 208-V, PF: 0.85, length: 30-cm, diameter: 25-cm, number of poles: 4. This case was simulated using FE shown in Fig. 10 (a).

The simulation was computed in six hours with 950000 elements and 5.7 million degrees of freedom. Since the case includes very small elements and also nonlinear materials, e.g., the core of the machine, the simulation of the inverter connected to the load or motor may take 8 hours or more for only one time instant.

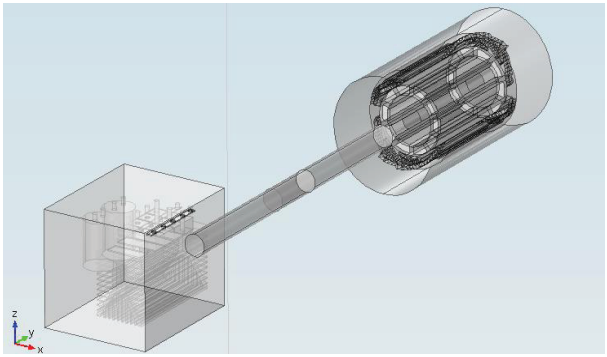

(a)

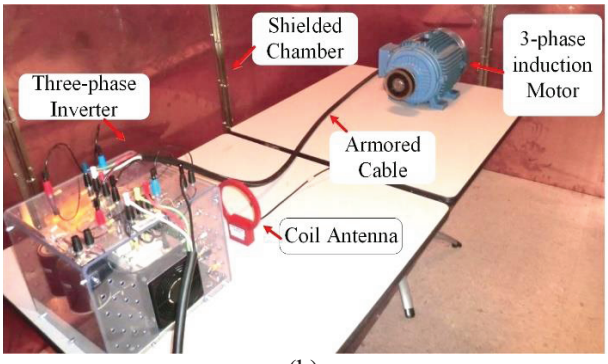

(b)

Fig. 10. The scheme of the setup of case 2: (a) FE simulation, and (b) measurement.

Generally, linear or non-linear solvers are being used in the FE simulations. In this case, since there are several materials with nonlinear characteristics, the linear solver cannot be used. On the other hand, using nonlinear material rises the simulation time dramatically. Hence, a modification in choosing the solver and the associated iterative technique was employed. Instead of having linear or curved commutation curve, the ramp of the curve in several zones was calculated (μ_{r1}, μ_{r2} …) and used instead of the commutation curve in this part, as shown in Table 2. The benefit of this modification is that the magnetic flux density of a component changes in a very small period due to the steady state condition of the system. For example, the magnetic flux density of the stator core of the induction motor is about 1.5-2 T in power frequency analysis, 50-60 Hz. For higher frequencies, it goes down to under 1 T. Therefore in this case, a specific zone of the permeability can be chosen for this component. Similarly, the permeability of the other components of the system can be chosen based on the working frequency. Therefore, having the idle parts of the commutation curves of the elements would be avoided and the simulation time decreases. This algorithm can be defined in the material properties part of the FE simulation.

Table 2: Commutation curve of some material used in the simulation

Material	Flux Density (T)	Permeability (μ)
Steel (μ_{r1})	0-1.2	1.2×10^{-3}
Steel (μ_{r2})	1.2-1.5	1.5×10^{-4}
Steel (μ_{r2})	1.5-1.8	4.2×10^{-5}
Iron	0.2-0.6	1.3×10^{-4}

In addition to the modification in defining the material properties, some modification needs to be performed for the solver to have a flexible solution. Hence, as the iterative solver, the fast generalized minimal residual technique, GMRES, with the Krylov's method as the pre-conditioner was used. The fast GMRES is a variant of the GMRES method with flexible preconditioning that enables the use of a different pre-conditioner at each step of the Arnoldi process. The Krylov subspace is a linear subspace which enables multi-preconditioning [17]. In particular, a few steps of GMRES can be used as a pre-conditioner for fast GMRES. The flexibility of this solution method is beneficial for the problem with nonlinear material characteristics such as the motor's core. Therefore, the simulation time decreases from about 8-9 hours to about 20 minutes. More explanation is given in [18].

In addition to the simulation, the experimental setup was implemented in a chamber which isolates the setup from the outside environment, shown in Fig. 10 (b). The experiment was implemented based on the

MIL-STD-462D [19]. The coil antenna and the real-time spectrum analyzer, which is used in the measurement, are specifically for low frequency analysis with high precision. The frequency range of the utilized coil antenna is between 20-Hz–500-kHz. The winding of the antenna is 36 turns of 7-41 litz wire shielded with 10 Ohms resistance and 340-μH inductance. The antenna and the setup were located based on the standards (MIL-461-STD [20], MIL-462-STD). The spectrum analyzer also covers 1-Hz-3–GHz with ±0.5 dB absolute amplitude accuracy to 3-GHz. The coil antenna was located at 10 cm away from the inverter to obtain the stray magnetic field. The fields were transferred to an EMI receiver, real-time spectrum analyzer, with a cable of 50-Ω impedance.

The magnetic field intensity (H-field) generated from the setup in simulation is shown in Fig. 11. The H-field at 5-kHz frequency is shown on a slice at 10 cm away from the setup, the same as experimental setup. As illustrated in this figure, the amplitude of the stray field around the inverter box is higher than other places. The reason is that the switching frequency of the inverter is 5 kHz, the same as the frequency depicted from the simulation figure. The simulation was implemented at several other frequencies. Only the switching frequency of the inverter which is 5-kHz, is shown here.

The setup was also implemented experimentally. The frequency response from DC to 20-kHz was obtained and shown in Fig. 12.

The unit of the simulation result is μA/m, while the unit of the experimental results is dBμA/m. The μA/m can be converted to dBμA/m by using eq. (7). Using this equation, the peak of the stray magnetic field at 5-kHz at the given distance is -4.37 dBμA/m experimentally, would be 0.61 μA/m which is very close to the value in simulation, see Fig. 11;

$$1\,\mu A/m = 10^{\frac{dB\mu A/m}{20}}. \quad (7)$$

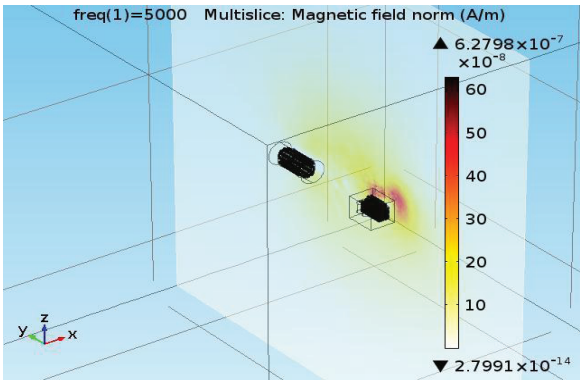

Fig. 11. Stray magnetic field intensity of the setup case 2 at 5 kHz simulated in FE (μA/m).

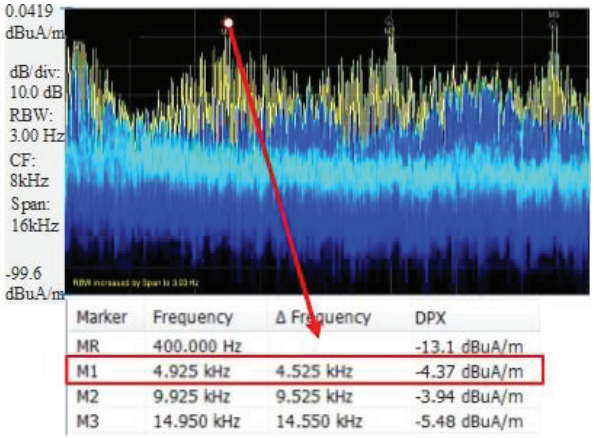

Fig. 12. Measured frequency response of the stray magnetic field intensity of the setup case 2 from DC to 20 kHz (dBμA/m).

IV. APPLICATIONS OF THE FREQUENCY RESPONSE ANALYSIS OF THE STRAY FIELD

Following the experimental verification of the simulation results, related applications such as monitoring of components for the diagnosis of failures and shielding were investigated:

As shown in Fig. 12, the first peak located at very low frequency is generated from the induction motor, since the motor is working at the power frequency, 60 Hz. As the working frequencies of the components in the system are different, the behavior of each component can be investigated individually. This can be a very useful hint in monitoring the conditions as well as detecting the faults of the motor and the inverter. For example in case 2, Fig. 12, if a failure occurs in the motor, the peak at the power frequency and the related higher harmonic orders will shift along the frequency band or the amplitudes would change. Similarly, failures to the inverter may cause the same type of changes in switching frequency and the related higher harmonic orders. Note that, the peaks at 10-kHz and 15-kHz in Fig. 12 are due to the second and the third harmonics of the inverter. The frequency responses in between the harmonics are noises and sub-harmonics.

As another application of this case, the shielding in the vicinity of the switch, 5 cm, was tested. Figure 13 shows the frequency response of the stray H-field with and without the shield between the switches and the antenna by means of simulation and measurement. Using a steel shield, Steel 1018, as an example in this test, it can be seen that the noises, sub-harmonics between the main harmonic orders, decrease dramatically. The experimental results show a wider band of frequency, DC–20 kHz, as shown in Fig. 14 to illustrate the effect of shielding on the other harmonic

orders.

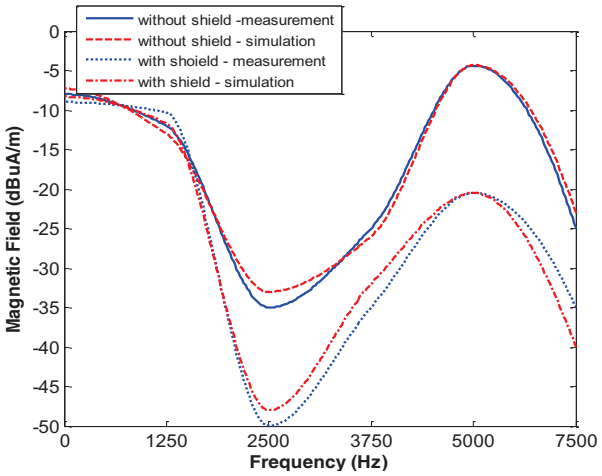

Fig. 13. Stray H-field of the case2 from DC-7.5 kHz (dBμA/m) at 5 cm from the inverter with and without shield by simulation and measurement.

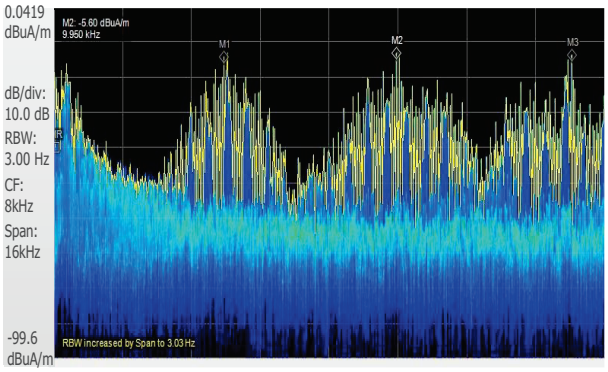

(a) Without shield

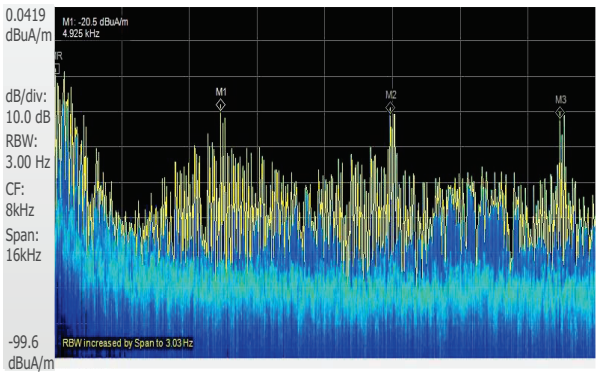

(b) With shield

Fig. 14. Stray H-field of the case 2 from DC-20 kHz (dBμA/m) at 5 cm away from the inverter: (a) without shield, and (b) with shield.

Consequently, considering this test, the main harmonics and the related sub-harmonics can help in selecting a shield with proper characteristics including the permittivity and permeability. Comparing the curves of Fig. 13, the simulation result is similar to the experimental one. Hence, the proposed shield can be studied and optimized using the physics based simulation. The permittivity, permeability, conductivity and other physical characteristics of the shield can be altered and optimized for the best electromagnetic compliance or any other purposes using simulation and experimental design.

V. CONCLUSION

In this paper, 3D full finite element modeling for the radiated EMI study of a typical power electronic drive was implemented. The physical approach for applying the switching activity was utilized. In order to have the detailed simulation of the model and simultaneously consider the non-linearity of commutation curve in the frequency analysis, the fast GMRES methods with proper pre-conditioners were used as the solution method which increases the simulation speed. The measurement was also applied for verification of the numerical results as well as for investigating the stray fields under different operating conditions. The results show that the FE model has a good accuracy for evaluating the stray fields. Two cases of using the inverter in the system were studied and their applications were explained. The results show that the frequency response of the field can be used for assessing shielding arrangements as well as for monitoring the conditions of the drive.

ACKNOWLEDGEMENTS

Part of this work was supported by a grant from the Office of Naval Research.

REFERENCES

[1] M. Halgamuge, C. D. Abeyrathne, and P. Mendis, "Measurement and analysis of electromagnetic fields from trams, trains, and hybrid cars," *Radiation Protection Dosimetry*, vol. 141, no. 3, pp. 255-268, 2010.

[2] M. Olofsson, "Low frequency EMC and power quality," *In Compliance Mag*., pp. 34-41, Apr. 2012.

[3] M. Olofsson and U. Grape, "Framework for electromagnetic compatibility in electric power systems," *VIII International Symposium and Exhibition on Electromagnetic Compatibility and Electromagnetic Ecology*, St. Petersburg, Russia, June 16-19, 2009.

[4] Electromagnetic Health Organization, "EMF test of 2007 Toyota Prius hybrid," *Electromagn. Health*, 2008.

[5] H. Akagi and T. Shimizu, "Attenuation of conducted EMI emissions from an inverter-driven

motor," *IEEE Transactions on Power Electronics*, vol. 23, pp. 282-290, 2008.
[6] N. Mutoh, J. Nakashima, and M. Kanesaki, "Multilayer power printed structures suitable for controlling EMI noises generated in power converters," *IEEE Transactions on Industrial Electronics*, vol. 50, no. 6, pp. 1085-1094, Dec. 2003.
[7] O. Aouine, C. Labarre, and F. Costa, "Measurement and modeling of the magnetic near field radiated by a buck chopper," *IEEE Transactions on Electromagnetic Compatibility*, vol. 50, no. 2, pp. 445-449, May 2008.
[8] M. R. Barzegaran and O. A. Mohammed, "3-D FE wire modeling and analysis of electromagnetic signatures from electric power drive components and systems," *IEEE Transactions on Magnetics*, vol. 49, no. 5, pp. 1937,1940, May 2013.
[9] G. Ala, M. C. Di Piazza, G. Tine, F. Viola, and G. Vitale, "Numerical simulation of radiated EMI in 42V electrical automotive architectures," *IEEE Transactions on Magnetics*, vol. 42, no. 4, pp. 879-882, Apr. 2006.
[10] Z. Cheng, H. Takahashi, B. Forghani, L. Liu, Y. Fan, T. Liu, J. Zhang, and X. Wang, "3-D finite element modeling and validation of power frequency multi-shielding effect," *IEEE Transactions on Magnetics*, vol. 48, pp. 243-246, Feb. 2012.
[11] A. Nejadpak and O. A. Mohammed, "Physics-based modeling of power converters from finite element electromagnetic field computations," *IEEE Transactions on Magnetics*, vol. 49, no. 1, pp. 567-576, Jan. 2013.
[12] F. T. Ulaby, *Fundamental of Applied Electromagnetics*, 5th Edition, Prentice Hall, pp. 321-324, 2006.
[13] N. N. Rao, *Elements of Engineering Electromagnetics*, 6th Edition, Prentice Hall, pp. 637, 2004.
[14] A. Nejadpak, B. Mirafzal, O. Mohammed, and L. Wei, "Effects of different switching algorithms on the thermal behavior of IGBT modules under pulse-load conditions," *IECON 2010-36th Annual Conference on IEEE Industrial Electronics Society*, vol., no., pp. 451-456, Nov. 7-10, 2010.
[15] D. C. Giancoli, *Physics: Principles with Applications*, Pearson Education, pp. 624, 2005.
[16] C. R. Paul, *Inductance: Loop and Partial*, Wiley-IEEE Press, pp. 195, 2011.
[17] W. E. Arnoldi, "The principle of minimized iterations in the solution of the matrix eigenvalue problem," *Quarterly of Applied Mathematics*, vol. 9, pp. 17-29, 1951.
[18] J. Stoer and R. Bulirsch, *Introduction to Numerical Analysis*, 3rd Edition, Springer, New York, 2002.
[19] MIL-STD-462D, *Measurement of Electromagnetic Interference Characteristics*, Aug. 20, 1999.
[20] MIL-STD-461F, *Requirements for the Control of Electromagnetic Interference Characteristics of Subsystems and Equipment*, pp. 91-98, Dec. 10, 2007.
[21] M. R. Barzegaran, A. Nejadpak, and O. A. Mohammed, "Evaluation of high frequency electromagnetic behavior of planar inductor designs for resonant circuits in switching power converters," *Applied Computational Electromagnetic Society (ACES) Journal*, vol. 26, no. 9, pp. 737-748, Sep. 2011.
[22] G. L. Skibinski, R. J. Kerkman, and D. Schlegel, "EMI emissions of modern PWM AC drives," *IEEE Industrial Application Magazine*, vol. 5, no. 6, pp. 47-80, 1999.
[23] O. Martins, S. Guedon, and Y. Marechal, "A new methodology for early stage magnetic modeling and simulation of complex electronic systems," *IEEE Transaction on Magnetics*, vol. 48, no. 2, pp. 319-322, 2012.

Mohammadreza Barzegaran (S'10) obtained his B.Sc. and M.Sc. degrees in Power Engineering from University of Mazandaran, Iran in 2007 and 2010 respectively. He defended his Ph.D. degree in the Department of Electrical and Computer Engineering, Florida International University, Florida, USA. He is now Assistant Professor at Lamar University. His research interests include studying electromagnetic compatibility in power components, life assessment of electrical power components, fault detection in electrical machines, and also computer-aid simulation of power components. He has many published papers in journals and conferences.

Arash Nejadpak received his B.S. degree in Electrical Engineering and his M.S. degree in Power Electronics and Electric Machines from Sharif University of Technology, Tehran, Iran, in 2007 and 2009, respectively. Currently, he is working towards the Ph.D. degree in Electrical Engineering at the Florida International University, Miami. His current research interests include intelligent control of PM machines and

development of physics-based models and design optimization of power electronic conversion systems. He has many published papers in international journals and conferences.

Osama A. Mohammed (S'79, M'83, SM'84, F'94): is a Professor of Electrical and Computer Engineering and the Director of the Energy Systems Research Laboratory at Florida International University. He received his M.S. and Ph.D. degrees in Electrical Engineering from Virginia Polytechnic Institute and State University. He published numerous journal articles over the past 30 years in areas relating to power systems, electric machines and drives, computational electromagnetics and in design optimization of electromagnetic devices, artificial intelligence applications to energy systems. He authored and co-authored more than 350 technical papers in the archival literature. He has conducted research work for government and research laboratories in shipboard power conversion systems and integrated motor drives. He is also interested in the application communication and wide area networks for the distributed control of smart power grids. He has been successful in obtaining a number of research contracts and grants from industries and Federal government agencies for projects related to these areas. Mohammed also published several book chapters including: Chapter 8 on Direct Current Machinery in the Standard Handbook for Electrical Engineers, 15th Edition, McGraw-Hill, 2007 and a book Chapter entitled "Optimal Design of Magnetostatic Devices: the Genetic Algorithm Approach and System Optimization Strategies," in the book entitled: Electromagnetic Optimization by Genetic Algorithms, John Wiley & Sons, 1999.

Mohammed is a Fellow of IEEE and is the recipient of the IEEE PES 2010 Cyril Veinott Electromechanical Energy Conversion Award. Mohammed is also a Fellow of the Applied Computational Electromagnetic Society. He is Editor of IEEE Transactions on Energy Conversion, IEEE Transactions on Magnetics, IEEE Transactions on Smart Grid and COMPEL. Mohammed was the past President of the Applied Computational Electromagnetic Society (ACES). He received many awards for excellence in research, teaching and service to the profession and has delivered numerous invited lectures at scientific organizations around the world.

Mohammed has been the general chair of several international conferences including; ACES 2006, IEEE-CEFC 2006, IEEE-IEMDC 2009, IEEE-ISAP 1996 and COMPUMAG-1993. He has also chaired technical programs for other major international conferences including; IEEE-CEFC 2010, IEEE-CEFC-2000 and the 2004 IEEE Nanoscale Devices and System Integration. Mohammed also organized and taught many short courses on power systems, Electromagnetics and intelligent systems in the U.S.A and abroad. Mohammed has served ACES in various capacities for many years. He also serves IEEE in various boards, committees and working groups at the national and international levels.